High Temperature Behaviour of Hercynite

I. Jastrzębska, J. Szczerba

Hercynite ($FeAl_2O_4$) was obtained by Arc Plasma Synthesis (APS) and thermally annealed at 1000 °C for 1, 24 and 36 h respectively, in air. The XRD measurements, that were conducted before and after the annealing, showed an evident alteration of the original hercynite under the influence of temperature and oxygen access. About half of the original hercynite was preserved after the longest annealing treatment of 36 h. The remained iron-aluminium spinel underwent decomposition into a few iron and aluminium oxide phases, among which non-stoichiometric magnetite and corundum were the most significant. Mössbauer spectroscopy showed that hercynite is a normal spinel with a slight inversion parameter of 11 %, which was increased up to 34 % after the 36 h thermal annealing. An overlapping of reflexes for spinel-like phases γ-Fe_2O_3 and γ-Al_2O_3 with Fe–Al spinel interfered with their detection by X-ray diffractometry. The Mössbauer spectroscopy measurements confirmed the presence of magnetite in the after-annealed samples. The electron probe microanalysis of the hercynite oxidised surfaces showed well-developed, scalenohedral morphology of the crystals, and well-defined compositions corresponding to Al-containing Fe_2O_3 measured by wavelength-dispersive X-ray spectroscopy. The results of XRD, MS and SEM/EPMA examinations lead to establishing a general oxidation mechanism of hercynite at high temperatures.

1 Introduction

Compounds with the spinel structure have attracted much scientific and technological attention, due to their beneficial physico-chemical and mechanical properties, both at ambient and elevated temperatures [1–10]. Hercynite, $Fe^{2+}Al_2O_4$, has advantageous properties like thermal resistance (melting temperatures: $T_{mFA} = 1780$ °C) [11], low thermal expansion coefficient ($\alpha_{1000\,°C,\ FA} = 0{,}85$ % [12]), high hardness and wear resistance [13]. On the other hand, hercynite as an Fe-endmember spinel mineral forms under earth's conditions of high temperature and pressure above 150 °C and 400 MPa, respectively [14]. Hence, the occurrence of hercynite does not relate to economically effective deposits, entailing today many industrial challenges to development of its synthesis [15, 16]. Synthesis of hercynite is difficult by means of the traditional solid-state reaction and requires, apart from the high temperature, above 1500 °C, also the well-controlled atmosphere, which enables Fe ions to accept or reveal electrons, so that to gain and remain at the 2+ oxidation state [15]. Furthermore, hercynite was tried to be obtained by other more advanced methods as high-energy-ball-milling [17] or by use of detonation and shock waves [18], but there were still some reagents left or undesired intermediate phases detected in the product after the synthesis.

It was previously reported [19] that the method of synthesis utilising arc plasma is highly suitable for obtaining, in very short time, a dense and monophasic material composed of pure Fe–Al spinel with satisfactory chemistry with respect to inversion parameter. Therefore this method was applied in this work. The Arc Plasma Synthesis (APS) belongs to the techniques of fast synthesis using direct current, in this case for melting of constituents, and is especially suitable for those materials which precursors are able to diffuse and react in a liquid state. It was reported that arc plasma melted materials are characterised by beneficial and relatively different microstructural and physicochemical properties [20–22] in comparison to those obtained by the traditional solid state reaction. Surprisingly, this issue is still scarcely explored in literature.

Hercynite, belonging to the spinel sensu lato oxide group with Fd3m symmetry

Ilona Jastrzębska, Jacek Szczerba
AGH University of Science and Technology
Faculty of Materials Science and Ceramics
Department of Ceramics and Refractories
30-059 Kraków
Poland

Corresponding author: *I. Jastrzębska*
E-mail: Ilona.jastrzebska5@gmail.com

Keywords: hercynite, $FeAl_2O_4$, spinel, structure

Received: 29.08.2018
Accepted: 26.09.2018

(227 space group number), adopts a normal cation distribution at low temperatures [23–26]. The normal cation distribution means that Fe^{2+} ions occupy 8 tetrahedral sites (out of 64 T_d sites), while Al^{3+} ions fill up 16 octahedral sites (out of 32 O_h sites) in the spinel unit cell. With increasing temperature, the order in the cation sublattice arrangement is affected, as cations in T_d and O_h sites start to exchange their positions. This phenomenon is called spinel inversion and is described by so-called inversion parameter x, which is the fraction of B ions that moved from O_h into T_d sites ($[A_{1-x}B_x]^{IV}[A_xB_{2-x}]^{VI}O_4$]). In the ideally inverse spinel structure all of the T_d sites are occupied by B ions, while O_h sites contain equal number of A and B cations. The x parameter for such a structure is equal to 1, whereas for the perfectly normal spinel x = 0 [12].

Lavina et al. [27] conducted the first time-temperature oxidation experiments on a synthetic Mg-hercynite solid solution $Fe^{2+}_{0,699}Mg_{0,301}Al_{1,941}Fe^{3+}_{0,059}O_4$ and revealed that only hercynite was involved in the oxidation reaction (the mixture was calculated as containing 70 % of hercynite, 27 % of spinel and 3 % of magnesioferrite). To the authors knowledge, the thermal behaviour of pure hercynite in air atmosphere has not been investigated yet by other authors using Mössbauer Spectroscopy and Scanning Electron Microscopy [26, 28, 29], thus needing to be explored for its industrial application as active and advanced refractory material [1, 22, 30–32]. This work aims to investigate hercynite spinel with a formula $(Fe^{2+}_{0,89}Al_{0,11})^{Td}[Al_{1,85}Fe^{3+}_{0,11}]^{Oh}O_4$ under the conditions of increased temperature in air atmosphere.

2 Experimental

Hercynite was synthesized through the arc-melting process using a stoichiometric mixture of pure analytical grade of ferric oxide and aluminium oxide as precursors. The mixture was homogenized and pressed into pellets of 20 mm before the arc plasma melting process.

The arc plasma synthesis method has been previously found to be an effective route in obtaining monophasic material composed of iron-aluminium spinel with a satisfactory stoichiometry [19, 33–34]. Therefore this method was applied in the present work.

The arc plasma synthesis (APS) [35, 36] was carried out in the arc furnace Speko-Arc300 (producer: Spaw-Projekt, www.spaw-projekt.com.pl), equipped with a water cooled copper crucible and a tungsten electrode. The synthesis was conducted in the inert gas environment of a pure argon (Ar) flow. After melting of the sample the arc plasma was ended and the material was left in the furnace to cool down with an approximate cooling rate of 15 °C/s in the first seconds.

The synthesized products consisted of black coloured crystals, which appeared deep-green after powdering. These distinguishing features were agreeable with the ones reported in [37, 23]. The arc plasma synthesized samples (H_0) were subsequently subjected to three different heating cycles at 1000 °C for 1 h, 24 h and 36 h (H_1, H_{24} and H_{36}, respectively) in air atmosphere.

The powdered run products were subjected to X-Ray Diffraction (XRD) analyses in order to confirm the presence of hercynite in the as-synthesized sample and the alterations in the after-annealing ones. The XRD measurements were collected at room temperature using PANanalytical X'Pert Pro MPD X-ray diffractometer, in Bragg-Brentano mode, with CuK_α radiation (λ = 1,54056 Å). The data were collected over a range 10–90° 2θ. The qualitative analyses were performed using X'Pert High Score Plus software. The quantitative analyses and determination of hercynite crystal structure, including determination of lattice and oxygen parameters, were performed using Rietveld refinements based on the collected X-ray diffraction data, applying Maud software [38].

Mössbauer spectroscopy (MS) measurements of the samples before and after annealing process were conducted in a transmission mode with the use of RENON MsAa-3 spectrometer equipped with the LND Kr-filled proportional detector and He–Ne laser based interferometer, used to calibrate the velocity scale. A commercial 57Co(Rh) source kept at room temperature was applied for 14,41-keV resonant transition in ^{57}Fe. All isomer shift data given are relative to α-Fe throughout this paper. The Mössbauer absorbers were prepared by mixing ~80 mg of the powdered sample with epoxy resin. Spectra were recorded at standard temperature, and the isothermal scans were collected with 1023 points per each spectrum.

Finally, the surface of the investigated materials was observed under the ultra-high definition Scanning Electron Microscope (SEM) Nova Nano SEM 200, equipped with an energy dispersive spectrometer EDS. Additionally, the Electron Probe Microanalyser (EPMA) JEOL JXA-8230 was used to identify the hercynite oxidation products. The samples for EPMA measurements were in the form of polished cross-sections prepared by a traditional ceramographic technique.

3 Results and discussion

3.1 XRD study

Fig. 1 demonstrates XRD patterns and results of the phase analyses for both the as-synthesized spinel sample (H_0) and for the after-annealing ones (H_1, H_{24}, H_{36}). The quantitative phase analyses and structure solution were extracted from Rietveld refinements. The Rietveld refinements were performed using Maud software [38] and the structural models (ISCD database) of all possible occurring secondary phases, which are marked in the diffractograms (Fig. 1) (JCPDS: (H) $FeAl_2O_4$ 01-082-0595, (αA) α-Al_2O_3 01-089-3072, (γA) γ-Al_2O_3 01-075-0278, (M) Fe_3O_4 04-017-1024). The XRD pattern for the H_0 (as-synthesized) sample showed its monophasic character, where all the registered reflexes were ascribed to hercynite of cubic symmetry (Fd3m space group), and this demonstrates the effectiveness of the arc plasma synthesis (APS) for Fe–Al spinel.

The diffractogram for H_{36} is significantly different when compared to the one of the starting (H_0) sample. It shows additional peaks and lower intensities of the reflections attributed to hercynite, while in the diffractogram of the H_1 only one reflex characteristic for magnetite appeared. The new reflexes in the H_{36} diffractogram were assigned to magnetite, α- and γ-alumina.

Tab. 1 presents hercynite spinel content in all the samples, hercynite and magnetite structure parameters, values of the unit cell volume determined by Rietveld refinement, together with the goodness of the fit. It can be observed from this table that the longer thermal treatment, the greater content of new phases in the after-annealing material. The XRD patterns refinement for

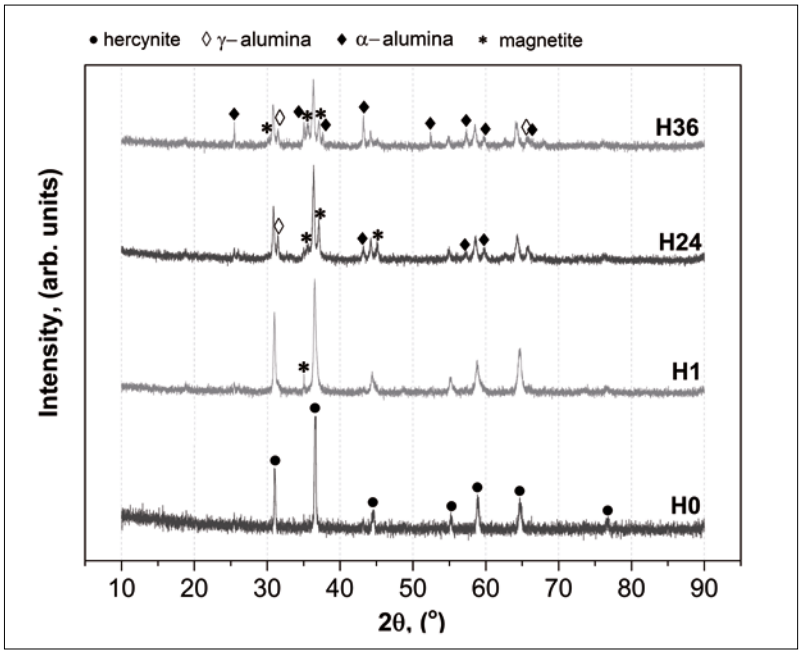

Fig. 1 XRD patterns for the as-synthesized sample of hercynite (H_0) and the after-annealing ones (H_1, H_{24} and H_{36})

longer time of annealing experiment is accompanied by the higher goodness of the fit. It shows that the quantitative analysis is less reliable, particularly in reference to the low content phases. While, the original untreated H_0 sample consisted of 100 % hercynite, the quantitative phase compositions for the annealed samples were as follows: H_1–(H) 98,2 %, (M) 1,8 %; H_{24}–(H) 64,4 %, (M) 14,1 %, (αA) 18,0 %, (γA) 3,5 %; H_{36}–(H) 50,2 %, (M) 16,5 %, (αA) 27,3 %, (γA) 6 %. With increasing annealing time the lattice parameters changed significantly from 8,1340 Å (H_0) to 8,1961 Å (H_{36}). Similarly, the oxygen positional parameter u showed the same trend, and increased with increasing annealing time from 0,262 up to 0,264 for H_1 and H_{36}, respectively.

The H_0 sample, which consisted only of hercynite, was characterised by the lattice parameter a = 8,1340(1) Å, while the theoretical a value for endmember $Fe^{2+}Al_2O_4$ is reported to be 8,1409 Å [39]. The lattice parameter obtained in this work for H_0 sample is close to the value reported in [40] with a = 8,125 Å. There are many discrepancies in the lattice and other structural parameters of hercynite published so far [25, 26, 28, 29, 41–43]. Available lattice parameter data for pure hercynite range from a = 8,096 Å [44] to 8,205 Å [6].

The main reason responsible for that may be a different thermal history of Fe-Al spinel gained after various synthesis processes followed by annealing or not. This affects the stoichiometry, which may deviate due to possible Fe^{3+} presence in hercynite structure as well as due to possible occurrence of cation vacancies.

The refined structure parameters a and u of hercynite are not consistent with those obtained by Lavina et al. [27], who oxidized Mg-hercynite solid solution with the formula $Fe^{2+}_{0,699}Mg_{0,301}Al_{1,941}Fe^{3+}_{0,059}O_4$. However, contrary to us they did not observe magnetite in their oxidation products. It is well known [28, 45, 46] that magnetite can dissolve in the hercynite structure at elevated temperatures above 870 °C, which may lead to an increase of the lattice parameter a [47].

The conducted Rietveld analysis revealed that almost half of the original spinel is preserved after the 36 h annealing treatment. It is associated with the progressive oxidation of hercynite during its heating in air, which proceeds presumably in steps, passing through different forms of $Fe(Al)_xO_y$ oxides.

Magnetite seems to be the main oxidation product of hercynite, present in the amount of 16,5 mass-% after the 36 h cycle. However, overlapping of reflexes in the diffractograms characteristic for Fe_3O_4 with reflexes of maghemite γ-Fe_2O_3 may play as a masking effect for the presence of this spinel-like compound in the sample. A similar situation occurs when analysing reflexes for γ-Al_2O_3, which also possesses the spinel-type cubic structure [48]. Nevertheless, the observed diffraction patterns found the exact match with the standards, so the presence of γ-alumina, magnetite and hercynite is evident.

Magnetite, detected by XRD was characterised by the higher lattice parameter of a = 8,373 Å (H_{36}, Tab. 1), which is very close to that obtained by [49]. It was previously reported that Fe_3O_4 may completely dissolve in $FeAl_2O_4$ at elevated temperatures above 1000 °C [45, 47]. Furthermore, Ritter et at. in the work [46] examined a homogeneous mixture of 50 % hercynite-50 % magnetite and determined an intermediate lattice parameter of the investigated solid solution with a = 8,31 Å (value between a for magnetite and hercynite). This explains the large values for the annealed hercynite obtained in the present study.

Tab. 1 Structure parameters and data for hercynite and magnetite obtained from Rietveld refinements

Sample	Hercynite Content [%]	a_h [Å]	u_h	V_h, [Å³]	a_m [Å]	Goodness of Fit
H_0	100	8,1340(1)	0,262(1)	538,2(1)	–	0,912
H_1	98,2	8,1492(2)	0,262(1)	541,2(1)	–	1,101
H_{24}	64,4	8,1890(6)	0,263(1)	549,2(3)	8,371(1)	1,251
H_{36}	50,2	8,1961(6)	0,264(1)	550,6(1)	8,368(1)	1,352

Indices: h = hercynite, m = magnetite

3.2 Mössbauer analysis

The obtained Mössbauer spectra for the samples H_0, H_{24} and H_{36}, demonstrated in Fig. 2, were fitted by assuming resonance lines of Lorentzian shape. The MS spectrum for the H_1 sample is comparable to the spectrum for the original H_0 sample. The refined hyperfine interactions parameters (HP) are compiled in Tab. 2.

The MS spectrum of the original H_0 sample was resolved into four quadrupole split doublets (D1, D2, D3 and D4). All of them were ascribed according to the values of the obtained isomer shifts (IS) as responsible for divalent (D1, D2 and D3) and trivalent (D4) iron in hercynite spinel. The average IS value for ferrous ions (Fe^{2+}) was 0,935 mm/s. Similar values for the isomer shift for $Fe^{2+}(T_d)$ were registered by Dézsi et al. [50] (in average 0,95 mm/s), and Larsson et al. [29] with mean IS = 1,075 mm/s. The higher value obtained in [29] could be explained by differences in the temperature during the measurements due to the temperature-dependent second-order Doppler shift [51]. All Fe^{2+} ions were attributed fully to the T_d positions but of three different symmetries, confirmed by three different values of quadrupole splitting (QS), which is proportional to bond symmetry of Fe atom [52]. The total contribution of ferrous ions in as-synthesized hercynite was 89,3 % with respect to Fe_{total} in hercynite.

The isomer shift of Fe^{3+} is much lower in comparison to IS for Fe^{2+} [52] therefore the last doublet designated as D4 (IS = 0,347 mm/s) is ascribed to Fe^{3+} in hercynite. An Fe^{3+} component in Fe-Al spinel was also previously observed by Larsson et al. [29] and Dézsi et al. [50] in their MS spectra, who reported IS = 0,47 mm/s, and IS = 0,30 mm/s for Fe^{3+}, respectively. Moreover, Fe^{3+} in hercynite was also reported elsewhere (Jastrzębska et al. [33, 34, 36, 53, 54], Lavina et al. [27]; Andreozzi and Lucchesi [25]. So, a low content of ferric ions commonly occurs in $FeAl_2O_4$.

According to the relative areas of Fe^{2+} and Fe^{3+} components in hercynite obtained by MS (Tab. 2), the stoichiometric formula of the as-synthesized starting hercynite (H_0) can be expressed as follows: $(Fe^{2+}_{0,89}Al_{0,11})[Fe^{3+}_{0,11}Al_{1,85}{}^{\square}_{0,04}]O_4$, where () and [] indicate T_d and O_h sites, respectively.

Because of the attribution of all the iron to hercynite spinel structure, the specified fraction of Al ions has to move from O_h into T_d sites and occupy them, which constitutes the inversion parameter x of the hercynite spinel. Accordingly, the relative fraction of Al in the O_h positions decreased, which together with the Fe^{3+} represent all the ions occupying this sites. For charge balancing of the hercynite formula, vacancies at this sites have been introduced. The appearance of

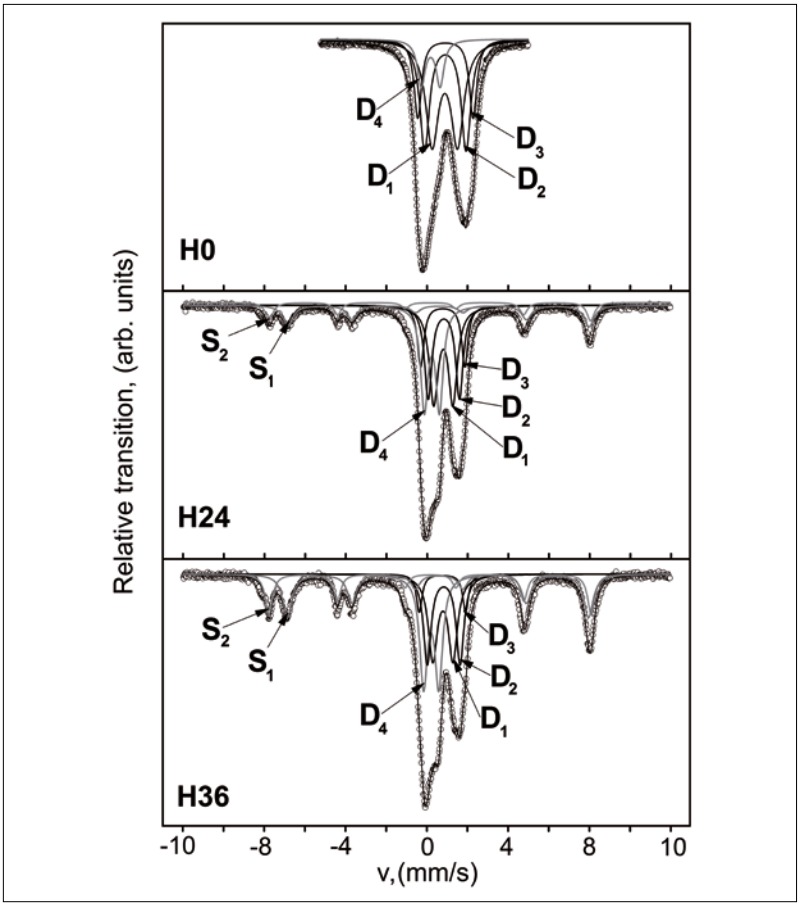

Fig. 2 Mössbauer spectra for the as-synthesized sample of hercynite (H_0), and the samples after thermal annealing (H_{24} and H_{36})

Tab. 2 MS hyperfine parameters for the as-synthesized hercynite (H_0), and the samples after annealing treatment (H_{24}, H_{36})

Sample	Component	IS [mm/s]	QS [mm/s]	Area [%]	Area [%]	Position Assignment	Magnetic Field [T]
H_0	D1	0,919(2)	1,033(9)	39,7(2)	89,3	Fe^{2+} (T_{d1}), H[1]	–
	D2	0,942(1)	1,681(8)	31,8(1)		Fe^{2+} (T_{d3}), H	
	D3	0,945(9)	2,242(8)	17,8(1)		Fe^{2+} (T_{d2}), H	
	D4	0,345(4)	0,758(7)	10,7(1)	10,7	Fe^{3+} (O_h), H	
H_{24}	D1	0,904(2)	0.950(18)	24,9(1)	57,7	Fe^{2+} (T_{d1}), H	–
	D2	0,929(1)	1,544(15)	20,6(3)		Fe^{2+} (T_{d2}), H	
	D3	0,877(3)	2,178(18)	12,2(1)		Fe^{2+} (T_{d3}), H	
	D4	0,337(4)	0,748(8)	22,1(2)	22,1	Fe^{3+} (O_h), H	
	S1	0,260(3)	≈0	8,03(1)	20,2	Fe^{3+} (T_d), M[2]	49,03
	S2	0,692(4)	≈0	12,17(1)		$Fe^{2,5+}$ (O_h), M	45,94
H_{36}	D1	0,897(4)	1,002(13)	19,4(1)	42,5	Fe^{2+} (T_{d1}), H	–
	D2	0,935(3)	1,622(10)	17,6(1)		Fe^{2+} (T_{d2}), H	
	D3	0,875(6)	2,286(11)	5,5(1)		Fe^{2+} (T_{d3}), H	
	D4	0,318(5)	0,749(9)	21,6(1)	21,6	Fe^{3+} (O_h), H	
	S1	0,277(5)	≈0	14,90(2)	35,9	Fe^{3+} (T_d), M	49,17
	S2	0.683(3)	≈0	21.00(2)		$Fe^{2,5+}$ (O_h), M	45,95

[1] hercynite, [2] magnetite, abbreviations: IS = isomer shift, QS = quadrupole splitting

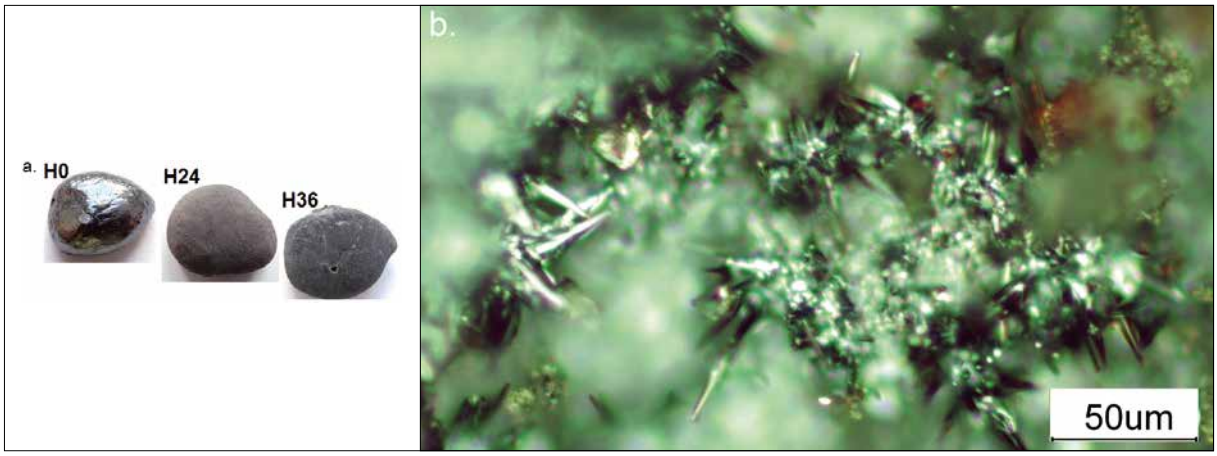

Fig. 3 a–b a) Macrostructure of the as-synthesized sample (H_0), and the samples after thermal annealing H_{24} and H_{36} sample; b) microstructure of the surface of H_{36} sample

vacancies in spinel compounds is energetically preferred in octahedral coordination [55–59].

The MS spectra of the after-annealing samples (H_{24} and H_{36}) significantly differ from the MS spectrum for the original H_0 sample. The main difference comes from the appearance of an additional sextet, with an increased area for the sample H_{36} compared to sample H_{24}, which may be due to the presence of a magnetically-ordered phase.

The procedure of fitting of the after-annealing spinel phases was analogical as for the H_0 sample, applying the previously fitted values of hyperfine interactions parameters (HP). Additionally, the change of IS in the following way $IS_{Fe3+}(T_d)<IS_{Fe3+}(O_h)<IS_{Fe2+}(T_d)<IS_{Fe2+}(O_h)$, given in [52], was utilised during interpretation of MS results.

After the thermal treatment, two new sextets (S1, S2), in both samples H_{24} and H_{36}, were observed in the MS spectrum, with average isomer shifts of $IS_{S1} = 0{,}269$ mm/s and $IS_{S2} = 0{,}688$ mm/s, which were ascribed to Fe^{3+} and $Fe^{2,5+}$, respectively. Additionally, the ratio of the relative areas S2/S1, which is 1,5 (H_{24}), showed that it is non-stoichiometric magnetite that appeared in the material after its high temperature exposure to air. The latter ion constitutes the average of Fe^{2+} and Fe^{3+} in the octahedral (O_h) site of magnetite, usually represented by the formula $[Fe^{3+}]^{Td}[Fe^{2,5+}]^{Oh}O_4$. Similar values of hyperfine parameters were obtained in [60] for magnetite annealed in air at 400 °C.

The ratio of iron atoms in the O_h to T_d sites equal to 1,5 for H_{24} and 1,4 for H_{36} indicates a nonstoichiometric composition of magnetite. Our MS results in combination with the results from XRD confirm the assumptions showed in [29] for possible hercynite decomposition products.

There are many MS studies concerning the structure and chemical environment of iron in magnetite, e.g. [59–61]. The values of HP for magnetite obtained in this study are very close to the ones obtained in [60] for the oxidized Fe_3O_4. The first component of the lower isomer shift (S1) was assigned to Fe^{3+} in the T_d sites, while the second component (S2) constituted an average for Fe^{2+} and Fe^{3+} in the O_h sites ($Fe^{2,5+}$) due to the fast electron exchange between these ions and resulting overlapping subspectra [59, 61]. Moreover, the obtained hyperfine magnetic fields strictly correspond to typical values for magnetite, being higher H = 49 T for the Fe^{3+} component and lower H = 46 T for the $Fe^{2,5+}$ component (H_{24}) [52, 60, 62]. The MS results are consistent with the XRD results confirming the presence of magnetite as a result of hercynite oxidation. Additionally, it should be noticed that HP for magnetite are relatively stable and remain almost the same after the second cycle of annealing (36 h treatment), but what significantly alters is the relative area of both the S1 and S2 components, which gives a total increase of the magnetite content from 20,2 % (H_{24}) up to 35,9 % (H_{36}). This behaviour is correlated with the decrease of the total relative area for iron component in Fe-Al spinel, that lowered from 57,7 % (H_{24}) to 42,5 % (H_{36}) with respect to the total iron content in the material.

The various values of QS for the three doublets (D1, D2 and D3), assigned to Fe^{2+} in hercynite, are associated with different bond symmetries of the tetrahedral Fe atom, with highest strain and asymmetry for a largest QS value, that is represented by the D3 component. This component is characterised by the QS above 2 mm/s for both H_{24} and H_{36} materials, and affects the largest decrease, approximately 55 % due to oxidation, dropping from 12,2 % (H_{24}) down to 5,5 % (H_{36}). Therefore it may be assumed that it mostly contributes to the formation of magnetite.

The contribution of ferric ions (Fe^{3+}) to the spectra of hercynite was fitted as a quadrupole doublet with isomer shift and quadrupole splitting which are typical for these ions occupying O_h sites in hercynite [29, 63] and other spinel compounds [52].

Since the area corresponding to the doublet D4 for Fe^{3+} is almost the same after 36 h annealing compared to 24 h cycle, it seems that Fe^{3+} stabilizes the hercynite structure at elevated temperatures and its influence on the formation of Fe_3O_4 is inconsiderable.

The area of the components ascribed to hercynite permitted to establish the approximate structural formulas of the after-annealing hercynites, that are as follows:

H_{24}: $(Fe_{0,72}Al_{0,28})[Fe_{0,28}Al_{1,63}{}^{\square}{}_{0,09}]O_4$;

H_{36}: $(Fe_{0,66}Al_{0,34})[Fe_{0,34}Al_{1,55}{}^{\square}{}_{0,11}]O_4$.

The increase in time of the thermal treatment results in a higher inversion parameter that raises from x = 11 % (H_0), through x = 28 % (H_{24}) up to x = 34 % (H_{36}). This behaviour is correlated with the increase of the fraction of vacancies at O_h sites [55] that form in order to balance the charge of the phase.

3.3 SEM/EPMA study

Fig. 3 a–b depicts the macroscopic view of the sample H_0 and the samples after annealing H_{24} and H_{36} as well as the microstructure of the surface of H_{36} sample. The original arc-plasma synthesized sample was characterised by a deep black colour and glossy, metallic surface (Fig. 3 a H_0). The macroscopic appearance of samples after thermal annealing shows that they significantly changed. The surface is no more glossy and smooth, but it is overgrown by crystals that made the samples very rough in touch (Fig. 3 a H_{24}, H_{36}).

The macroscopic appearance of the 1 h heat-treated sample (H_1) was not attached due to the slight macroscopic changes. Nevertheless, the influence of such short thermal treatment can be seen in Fig. 4 a–e. Fig. 4 b–c show that after the 1 h cycle at 1000 °C the hercynite crystals underwent decomposition. This decomposition is followed by creating the new non-well-formed and small micrometric crystals with a few sharp exhibited in Fig. 4 d of their size about 10 µm, and many of them covering uniformly the surface in Fig. 4 e. The EDS measurements in various regions of the decomposing hercynite crystal (Fig. 4 b) gave the compositions presented in Tab. 3. These points are numbered according to their increasing O/(Fe+Al) ratio reaching the maximum value of 1,79 in point 4, which is enriched in Fe, and minimum ratio in point 1 enriched in Al.

The longer thermal treatment revealed a privileged growth of the new crystals at the grain boundaries, which was demonstrated for the 24 h thermal cycle in Fig. 5 a–e. It can be observed that the sample H_{24} is covered by a branch chain of new crystals, forming particularly at the surfaces of the hercynite spinel material that constitute the grain boundaries.

Within the area of the grain boundaries the new crystals of characteristic needle shape morphology can be observed, which caused the very rough feeling when touching the sample.

The sharp crystals occurring at grain boundaries gathered with each other in clusters, and they were significantly larger at triple points (TP). The largest crystals at TP reach 100–120 µm, while their average size at boundaries is about 50 µm. On the other hand, the area within the grains is also overgrown, but with small reorganizing crystals, among which a single developing crystals of needle morphology can be observed (in the circle at Fig. 5 b–c).

After 36 h of the oxidation treatment the sample was almost completely covered on its whole surface. Fig. 6 presents microstructure developed during the 36 h thermal cycle with visible uniformly distributed sharp crystals. Fig. 6 b shows the layer-by-layer growth of the individual scalenohedral crystal.

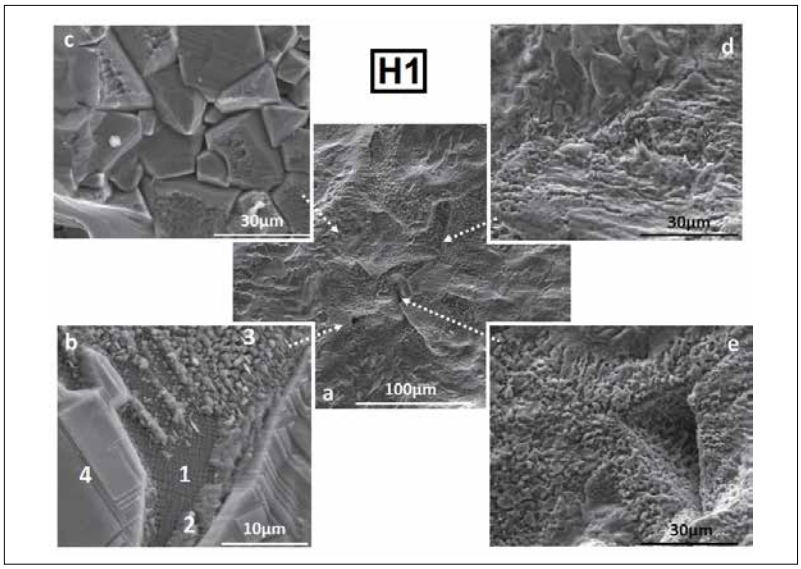

Fig. 4 Microstructure of hercynite sample after 1 h thermal treatment at 1000 °C (H_1)

Tab. 3 Results of EDS analysis in microareas of the sample H_1

Microarea	Element Content [at.-%]			Ratio of Elements	
	Fe	Al	O	O/Fe	O/Σ (Fe+Al)
1	16,0	23,6	60,4	3,8	1,53
2	22,5	16,6	60,9	2,7	1,56
3	21,5	14,7	63,8	3,0	1,76
4	23,0	12,8	64,2	2,8	1,79

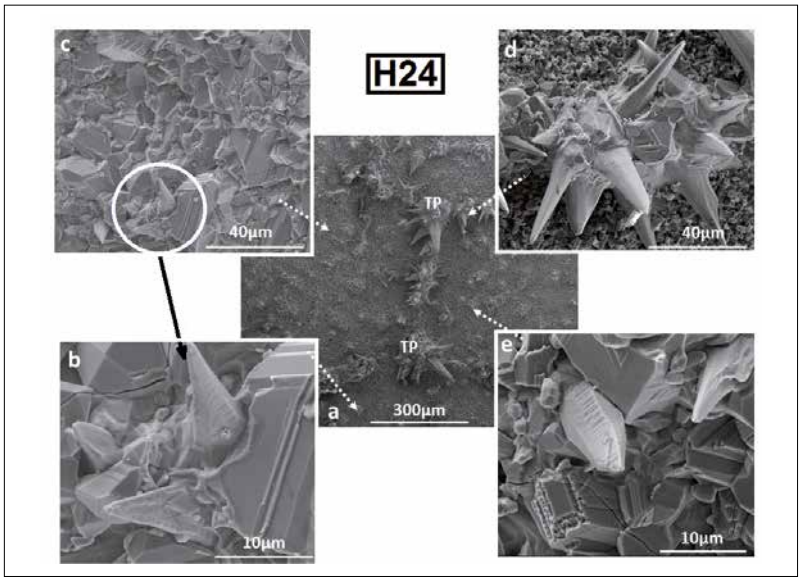

Fig. 5 a–e Microstructure of hercynite sample after 24 h thermal treatment at 1000 °C (H_{24})

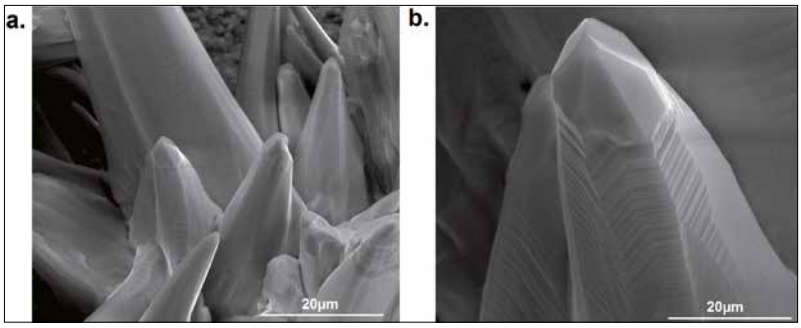

Fig. 6 Microstructure of hercynite sample after 36 h thermal annealing at 1000 °C (H_{36})

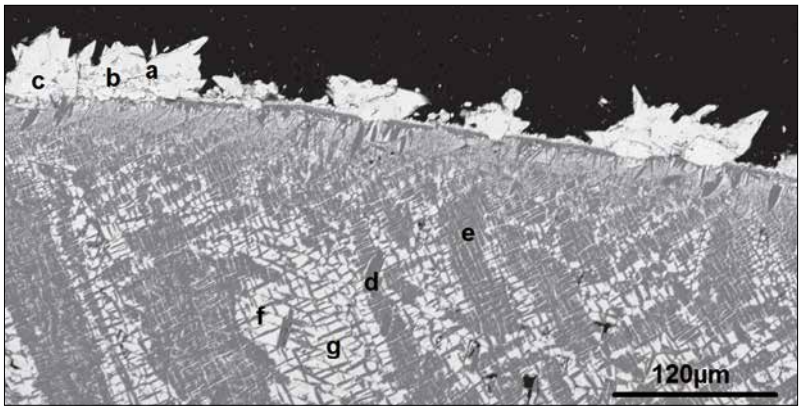

Fig. 7 SEM/EPMA microphotograph of the cross-section of the annealed sample H_{36}

Because magnetite possesses regular symmetry, trigonal scalenohedron morphology is unlikely to accept by magnetite, therefore we suggest hematite to constitute the elongated scalenohedral crystals. This type of symmetry of the crystal belongs to the hexagonal crystallographic system and is typical for calcite [64–66]. However, it is a rare morphology and especially unusual for hematite. Nevertheless, scalenohedron symmetry is agreeable with the hexagonal crystal symmetry of hematite [67].

In order to confirm the presence of hematite EMPA measurements were conducted on the cross-sections of the sample H_{36}. The image of the microstructure, together with the points where the WDS microanalyses were performed, is presented in Fig. 7. The analyses are compiled in Tab. 4.

Tab. 4 Representative WDS quantitative analysis in microareas of the sample H_{36}

	Microarea Composition [mass-%]						
	a	**b**	**c**	**d**	**e**	**f**	**g**
Al_2O_3	4,981	4,836	5,001	88,454	90,336	17,107	12,065
Fe_2O_3	95,494	95,271	94,865	11,680	9,693	49,273	54,649
FeO	0	0	0	0	0	34,218	33,084
Total	100,475	100,107	99,866	100,134	100,029	100,598	99,787
	Content of Ions [apfu[1]]						
Al^{3+}	0,151	0,147	0,153	1,844	1,872	0,704	0,514
Fe^{3+}	1,849	1,853	1,847	0,156	0,128	1,296	1,486
Fe^{2+}	0	0	0	0	0	1,000	1,000
O^{2-}	3	3,000	3	3,000	3,000	4,000	4,000
Fe^{2+}/Fe_{total}[2]	0	0	0	0	0	0,436	0,402
Chemical formula[3]	Al-containing hematite $Fe^{3+}_{1,85}Al_{0,15}O_3$			Fe-containing alumina $Al_{1,86}Fe^{3+}_{0,14}O_3$		Hercynite-magnetite s.s.[4] $Fe^{2+}Fe^{3+}_{1,39}Al_{0,61}O_4$	

[1] apfu = atoms per formula unit, [2] calculated by stoichiometry, [3] chemical formulas corresponding to average contents of ions, [4] solid solution

The measurement conducted in points a, b and c, which correspond to the needle-shape crystals observed previously by EDS (Fig. 6), showed an evident presence of Al-containing hematite. The dark areas, represented by points d and e, were attributed according to the WDS analysis to Fe-bearing alumina, while the brighter microareas presented by points f and g corresponded to Al-containing magnetite.

Some small inclusions of hematite (α-Fe_2O_3) in an artificially oxidized Al-Mg-Fe natural spinel annealed at 1150 °C were reported in [55] and confirmed in [68] as exsolution products. The inclusions were described as needle-like in shape, but no microstructural images were shown in this and any other study.

The general mechanism of oxidation proposed in [55] seems to work well in the case of hercynite. Special attention should be paid to the unusual morphology of the oxidation product that is supposed to be hematite. The numerous morphologies of hematite like hexagonal plates [69], spheres, cubes [70], spindles, rods, ellipsoids discs, stars, peanuts and others [71] are described as possible morphology of hematite. However, the literature reporting on non-typical scalenohedral symmetry of α-Fe_2O_3 is scarce. The only scientific report on the scalenohedral hematite was published recently by Makovicky et al. [72]. Neither XRD nor MS results, collected in this work, do detected hematite in the samples, presumably because of its low content in the sample. Hovever, it was possible to detect it by SEM/EPMA measurements in this study. The presence of αFe_2O_3 as the effect of magnetite oxidation is confirmed by other publication [60].

4 Conclusions

The APS method was found to be the effective route to obtain pure and highly crystalline hercynite with satisfactory cation ordering, low inversion parameter x = 0,11 and dense microstructure.

Hercynite, when subjected to thermal annealing decomposes stepwisely. The first step of annealing results in a formation

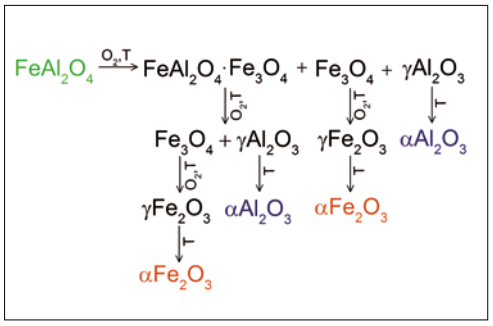

Fig. 8 Model of hercynite decomposition in air

of hercynite-magnetite s.s., magnetite and gamma-alumina. In the next step, solid solution separates by exsolution of magnetite and gamma-alumina. Then oxides undergoes oxidation or thermal transformation into more thermodynamically stable phases. Magnetite oxidizes into maghemite, which transforms into hematite, while gamma-alumina transforms into the most thermodynamically stable alpha-alumina. Therefore, the final oxidation products of hercynite are alpha-alumina and hematite of non-typical scalenohedral morphology.

Acknowledgements

The authors wish to express gratitude to the Spaw-Projekt Company/PL for assistance during arc plasma synthesis and input into the synthesis conditions settings.
The work was supported by the statutory funds of the Faculty of Materials Science and Ceramics, AGH University of Science and Technology.

References

[1] Liu, G.; et al.: Composition and microstructure of a periclase-composite spinel brick used in the burning zone of a cement rotary kiln. Ceram. Int. **40** (2014) [6] 8149–8155

[2] Rodríguez, E.; et al.: Hercynite and magnesium aluminate spinels acting as a ceramic bonding in an electrofused MgO–$CaZrO_3$ refractory brick for the cement industry. Ceram. Int. **38** (2012) [8] 6769–6775

[3] Liu, G.; et al.: Composition and structure of a composite spinel made from magnesia and hercynite. J. Ceram. Process. Res. **13** (2012) [4] 480–485

[4] Yan, D.; et al.: Reaction products and their solidification process of the plasma sprayed Fe_2O_3–Al composite powders. Mater. Chem. Phys. **133** (2012) [1] 190–196

[5] Scheffe, J.R.; Li, J.; Weimer, A.W.: A spinel ferrite/hercynite water-splitting redox cycle. Int. J. Hydrogen Energy **35** (2010) [8] 3333–3340

[6] Fukushima, J.; Hayashi, Y.; Takizawa, H.: Structure and magnetic properties of $FeAl_2O_4$ synthesized by microwave magnetic field irradiation. J. Asian Ceram. Soc. **1** (2013) [1]

[7] Wang, S.F.; et al.: Transparent ceramics: Processing, materials and applications. Prog. Solid State Chem. **41** (2013) [1–2] 20–54

[8] Wiglusz, R.J.; et al.: Hydrothermal preparation and photoluminescent properties of $MgAl_2O_4$:Eu^{3+} spinel nanocrystals. J. Lumin. **130** (2010) [3] 434–441

[9] Kruk, A.; et al.: $Mn_{1,5}Co_{1,5}O_4$ spinel conducting coatings on AL453 ferritic steel with regard to their application as interconnects in IT-SOFC. Arch. Metall. Mater. **58** (2013) [2] 377–381

[10] Lodha, R.; Troczyński, T.; Oprea G.: Role of oxide additives in the synthesis and sintering of magnesium aluminate spinel. Int. Ceramic Rev. **57** (2008) [5] 324–329

[11] Mao, H.; Selleby, M.; Sundman, B.: A re-evaluation of the liquid phases in the CaO–Al_2O_3 and MgO–Al_2O_3 systems. Calphad Comput. Coupling Phase Diagrams Thermochem. **28** (2004) [3] 307–312

[12] Grimes, N. W.: The spinels: Versatile materials. Phys. Technol. **6** (1975) [1] 22–27

[13] Santanach, J.G.; et al.: Mechanical and tribological properties of Fe/Cr–$FeAl_2O_4$–Al_2O_3 nano/micro-hybrid composites prepared by spark plasma sintering. Scr. Mater. **64** (2011) [8] 777–780

[14] Shulters, J.C.; Bohlen, S.R.: The stability of hercynite and hercynite-gahnite spinels in corundum- or quartz-bearing assemblages. J. Petrol. **30** (1989) [4] 1017–1031

[15] Chen J., et al.: Synthesis of hercynite by reaction sintering. J. Europ. Ceram. Soc. **31** (2011) [3] 259–263

[16] Robin, G.: Igneous rocks and processes. Hoboken, USA, 2010

[17] Botta, P.M.; Aglietti, E.F.; Porto López, J.M.: Mechanochemical synthesis of hercynite. Mater. Chem. Phys. **76** (2002) [1] 104–109

[18] Apolenis, A.; et al.: Synthesis of iron aluminates and a new modification of alumina at impact of explosive. Cent. Europ. J. Energ. Mater. **5** (2008) [3–4] 37–44

[19] Jastrzębska, I.; et al.: Crystal structure and Mössbauer study of $FeAl_2O_4$. Nukleonika **60** (2015) [1]

[20] Paesano, A.; et al.: Synthesis and characterization of Fe–Al_2O_3 composites. J. Magn. Magn. Mater. **264** (2003) [2–3] 264–274

[21] Jorg, S.; Gelbmann, G.; Krischanitz, R.: Ankral Q2 – an innovative solution for transition zones. RHI Bull. **2** (2012) 8–11

[22] Szczerba, J.; Jet al.: Corrosion of basic refractories in contact with cement clinker and kiln hot meal. J. Mater. Sci. Chem. Engin. **2** (2014) [10] 16–25

[23] Bowles, J.F.W.; et al.: Non-silicates: Oxides, hydroxides, and sulphides. Rock-forming Minerals, London 2011, 577–579

[24] Hill, R.J.; Craig, J.R.; Gibbs, G.V.: Systematics of the spinel structure type. Phys. Chem. Miner. **4** (1979) [4] 317–339

[25] Andreozzi, G.B.; Lucchesi, S.: Intersite distribution of Fe^{2+} and Mg in the spinel (sensu-stricto)-hercynite series by single-crystal X-ray diffraction. Amer. Mineral. **87** (2002) [8–9] 1113–1120

[26] Harrison, R.J.: The temperature dependence of the cation distribution in synthetic hercynite ($FeAl_2O_4$) from in-situ neutron structure refinements. Amer. Mineral. **83** (1998) [9–10] 1092–1099

[27] Lavina, B.; Princivalle, F.; Della Giusta, A.: Controlled time-temperature oxidation reaction in a synthetic Mg-hercynite. Phys. Chem. Miner. **32** (2005) [2] 83–88

[28] Harrison, R.J.; Putnis, A.: The magnetic properties and crystal chemistry of oxide spinel solid solutions. Surv. Geophys. **19** (1998) [6] 461–520

[29] Larsson, L.; O'Neill, H.S.C.; Annersten, H.: Crystal chemistry of synthetic hercynite (Fe-Al_2O_4) from XRD structural refinements and Mössbauer spectroscopy. Europ. J. Mineral. **6** (1994) 39–51

[30] Rodríguez, E.A.; et al.: Effect of hercynite spinel content on the properties of magnesia-calcium zirconate dense refractory composite. J. Europ. Ceram. Soc. **35** (2015) [9] 2631–2639

[31] Chen, J.; et al.: The kiln coating formation mechanism of MgO–$FeAl_2O_4$ brick. Ceram. Int. **42** (2016) [1] 569–575

[32] Geith, M.; Majcenovic, C.; Wiry, A.: Hercynite and galaxite – Active spinels, additives for excellent cement rotary kiln bricks. RHI Bull. **1** (2003) 25–29

[33] Jastrzębska, I.; et al.: Structural properties of Mn-substituted hercynite. Nukleonika **62** (2017) [2]

[34] Jastrzębska, I.; Szczerba, J.; Stoch, P.: Structural and microstructural study on the arc-plasma synthesized (APS) $FeAl_2O_4$–$MgAl_2O_4$

transitional refractory compound. High Temp. Mater. Process. **36** (2017) [3] 299–303

[35] Jastrzębska, I.; Szczerba, J.: Non-conventional method of ceramic preparation – arc plasma synthesis (APS). Proc. of the X Krakow Conf. of Young Scientists, Kraków 2015

[36] Jastrzębska, I.; Szczerba, J.; Stoch, P.: Structural and microstructural study on hercynite and its solid solutions. Proc. of 14th Bienn. Worldwide Congr. UNITECR'15, Wien 2015

[37] Hålenius, U.; Skogby, H.; Andreozzi, G.B.: Influence of cation distribution on the optical absorption spectra of Fe^{3+}-bearing spinel s.s.-hercynite crystals: Evidence for electron transitions in $VIFe^{2+}$-$VIFe^{3+}$clusters. Phys. Chem. Miner. **29** (2002) [5] 319–330

[38] Lutterotti, L.; Matthies, S.; Wenk, H.R.: MAUD: a friendly Java program for material analysis using diffraction. Universita degli Studi di Trento and University of California at Berkeley (1999) [21] 1–20

[39] Sickafus, K.E.; Wills, J.M.; Grimes, N.W.: Spinel compounds: Structure and properties relations. J. Amer. Ceram. Soc. **82** (1999) 3279–3292

[40] Hoffmann, A.; Fischer, W.A.: Bildung des Spinells $FeO{\cdot}Al_2O_3$ und seiner Mischkristalle mit Fe_3O_4 und Al_2O_3. Z. f. Phys. Chemie **7** (1956) [1–2] 80–90

[41] Krause, O.; Werner, T.: Zur Frage der Struktur einiger aluminiumoxydhaltiger keramischer Farbkörper. Z. f. Anorg. und Allg. Chemie **203** (1931) [1] 120–128

[42] Slack, G.A.: $FeAl_2O_4$–$MgAl_2O_4$: Growth and some thermal, optical, and magnetic properties of mixed single crystals. Phys. Rev. **134** (1964) [5A] 1268–1279

[43] Woodland, A.B.; Wood, B.J.: The breakdown of hercynite at low f_{O2}. Amer. Mineral. **75** (1990) [11–12] 1342–1348

[44] Yagnik, C.M.; Mathur, H.B.: A Mössbauer and X-ray diffraction study on the cation distribution in $FeAl_2O_4$. J. Phys. C Solid State Phys. 1968

[45] Turnock, A.C.; Eugster, H.P.: Fe–Al oxides: Phase relationships below 1000 °C. J. Petrol. **3** (1962) [3] 533–565

[46] Ritter, H.; et al.: Investigation of the demixing process in the system Fe_3O_4 (magnetite)–$FeAl_2O_4$. Diffus. Fundam. **12** (2010) [64]

[47] Schollenbruch, K.; Woodland, A.B.: The stability of hercynite at high pressures and temperatures. Phys. Chem. Miner. **37** (2010) 137–143

[48] Wefers, K.; Misra, C.: Oxides and hydroxides of aluminum. Alcoa Research Laboratories, 1987

[49] Sasaki, S.: Radial distribution of electron density in magnetite, Fe_3O_4. Acta Crystallogr. Sect. B Struct. Sci. **53** (1997) [5] 762–766

[50] Dézsi, I.; Szucs, I.; Sváb, E.: Mössbauer spectroscopy of spinels. J. of Radioanalytical and Nuclear Chem. **246** (2000) [1] 15–19

[51] Shrivastava, K.N.: Temperature dependence of the Mössbauer isomer shift. Hyperfine Interact. **26** (1985) [1–4] 817–843

[52] Greenwood, N.N.; Gibb, T.C.: Iron oxides and sulphids. Mössbauer spectroscopy, 1971, 239–303

[53] Jastrzębska, I.; Szczerba, J.: Synthesis of Fe–Al spinel with superior storage and transportation properties, Logistyka, no. 4, 9030–9037

[54] Jastrzębska, I.; Szczerba, J.: Elevated temperature electronic properties of hercynite spinel $FeAl_2O_4$ obtained by arc plasma synthesis (APS). Proc. of the Electronic Mater. and Appl. 2017, Orlando, USA

[55] Menegazzo, G.; Carbonin, S.; Della Giusta, A.: Cation and vacancy distribution in an artificially oxidized natural spinel. Miner. Mag. **61** (1997) [406] 411–421

[56] Sheldon, R.; et al.: Cation disorder and vacancy distribution in nonstoichiometric magnesium aluminate spinel, $MgO{\cdot}Al_2O_3$. J. Amer. Ceram. Soc. **82** (1999) [12] 3293–3298

[57] Jagodzinski, H.; Saalfeld, H.: Kationenverteilung und Strukturbeziehungen in Mg–Al-Spinellen. Z. f. Krist. New Cryst. Struct. **110** (1958) [1–6] 197–218

[58] Ferguson, G.A.; Hass, M.: Magnetic structure and vacancy distribution in γ-Fe_2O_3 by neutron diffraction. Phys. Rev. **112** (1958) [4] 1130–1131

[59] Daniels, J.M.; Rosencwaig, A.: Mössbauer spectroscopy of stoichiometric and non-stoichiometric magnetite. J. Phys. Chem. Solids **30** (1969) [6] 1561–1571

[60] Da Costa, G.M.; et al.: Influence of nonstoichiometry and the presence of maghemite on the Mössbauer spectrum of magnetite clays. Clay Miner. **43** (1995) [6] 656–668

[61] Gorski, C.A.; Scherer, M.M.: Determination of nanoparticulate magnetite stoichiometry by Mössbauer spectroscopy, acidic dissolution, and powder X-ray diffraction: A critical review. Amer. Mineral. **95** (2010) [7] 1017–1026

[62] Muramatsu, H.; et al.: Mössbauer spectroscopy of magnetite microcrystals dispersed in a polyvinyl alcohol film. Hyperfine Interact. **84** (1994) [1] 539–544

[63] Waerenborgh, J.C.; et al.: Powder XRD structure refinements and 57Fe Mossbauer effect of synthetic $Zn_{1-x}Fe_xAl_2O_4$ ($0<x\leq1$) spinels annealed at different temperatures. Phys. Chem. Miner. **21** (1994) [7] 460–468

[64] García Carmona, J.; Gómez Morales, J.; Rodríguez Clemente, R.: Rhombohedral-scalenohedral calcite transition produced by adjusting the solution electrical conductivity in the system $Ca(OH)_2$–CO_2–H_2O. J. Colloid Interface Sci. **261** (2003) [2] 434–440

[65] Thriveni, T.; et al.: Factors affecting the crystal growth of scalenohedral calcite by a carbonation process. J. Korean Ceram. Soc. **51** (2014) [2] 107–114

[66] Patel, A.R.; Patel, R.P.: Kurze Originalmitteilung: Etching of cleavages of calcite of scalenohedral habit. Z. für Krist. – New Cryst. Struct. **123** (1966) [2] 153–158

[67] Mandarino, J.A.; Anderson, V.: Monteregian treasures: The minerals of Mont-Saint-Hilaire, Quebec. New York1989

[68] Menegazzo, G.; Carbonin, S.: Oxidation mechanisms in Al–Mg–Fe spinels. A second stage: α-Fe_2O_3 exsolution. Phys. Chem. Miner. **25** (1998) [8] 541–547

[69] Liu, Z.C.; Zheng, Y.J.: Hexagonal hematite platelets synthesized from pyrite cinders by hydrothermal process. J. Cent. South Univ. Technol. English Ed. **18** (2011) [5] 1377–1382

[70] Jia, B.; Gao, L.: Growth of well-defined cubic hematite single crystals: Oriented aggregation and Ostwald ripening. Cryst. Growth Des. **8** (2008) [4] 1372–1376

[71] Cornell, R.M.; Schwertmann, U.: The iron oxides: Structure, properties, reactions, occurences and uses. Weinheim 2003

[72] Makovicky, E.; Parisatto, M.; Højlund F.: Non-destructive investigation of a scalenohedral hematite pendant from Bahrain, c. 1800 bc. Archaeometry **57** (2015) [1] 163–176